

Article pubs.acs.org/JACS

Single-Electron Currents in Designer Single-Cluster Devices

Suman Gunasekaran, Douglas A. Reed, Daniel W. Paley, Amymarie K. Bartholomew, Latha Venkataraman,* Michael L. Steigerwald,* Xavier Roy,* and Colin Nuckolls*



Cite This: J. Am. Chem. Soc. 2020, 142, 14924-14932



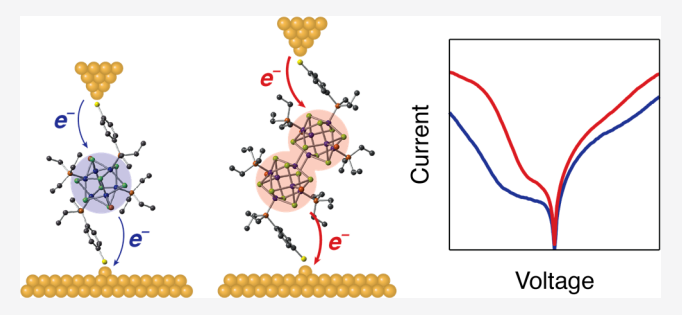
ACCESS

Metrics & More

Article Recommendations

Supporting Information

ABSTRACT: Atomically precise clusters can be used to create single-electron devices wherein a single redox-active cluster is connected to two macroscopic electrodes via anchoring ligands. Unlike single-electron devices comprising nanocrystals, these cluster-based devices can be fabricated with atomic precision. This affords an unprecedented level of control over the device properties. Herein, we design a series of cobalt chalcogenide clusters with varying ligand geometries and core nuclearities to control their current-voltage (I-V) characteristics in a scanning tunneling microscope-based break junction (STM-BJ) device. First, the device geometry is modified by precisely positioning



junction-anchoring ligands on the surface of the cluster. We show that the I-V characteristics are independent of ligand placement, confirming a sequential, single-electron tunneling mechanism. Next, we chemically fuse two clusters to realize a larger cluster dimer that behaves as a single electronic unit, possessing a smaller reorganization energy and more accessible redox states than the monomeric analogues. As a result, dimer-based devices exhibit significantly higher currents and can even be pushed to current saturation at high bias. Owing to these controllable properties, single-cluster junctions serve as an excellent platform for exploring incoherent charge transport processes at the nanoscale. With this understanding, as well as properties such as nonlinear I-V characteristics and rectification, these molecular clusters may function as conductive inorganic nodes in new devices and materials.

INTRODUCTION

A prototypical single-electron device comprises a nanoscale quantum dot isolated from the leads by tunnel junctions. 1-3 Current is driven by sequentially charging and discharging the quantum dot one electron at a time. Single-electron devices can serve as nanoscale circuit elements, such as transistors and switches, 4,5 and can be incorporated into novel quantum devices that require single-electron manipulations. 6-9 Conventional single-electron devices are fabricated lithographically; this limits both the miniaturization and the chemical uniformity of the quantum dots. Since single-electron devices require the energy level spacing of the quantum dot to be larger than the thermal energy ($\Delta E \gg k_B T$), conventional single-electron devices can only operate at low temperatures. Room temperature operation requires quantum dot sizes below ten nanometers to achieve sufficient energy level spacing. 10,11 This can be achieved with scanning probe patterning 12,13 or through the use of nanocrystals. 11,14–17 However, these approaches lack the requisite control over the properties of the quantum dot and the tunnel junctions needed for reproducible operation across several devices.

Single-molecule circuits can overcome these limitations since the quantum dot and the tunnel junctions can be defined with atomic precision using synthetic chemistry. 18-21 Although single-electron transfer processes at the molecular level have recently garnered significant interest, 22-24 room temperature

demonstrations of single-electron devices using single molecules are limited. 25-28 The reason for this dearth is that singlemolecule circuits typically comprise organic molecules or organometallic complexes²⁹ whose transport is dominated by coherent tunneling pathways.³⁰ As a result, even for redoxactive molecules,^{31–33} charging/discharging processes are overwhelmed by through-bond tunneling across the molecular junction.³⁴

In contrast, redox-active atomically precise inorganic clusters^{38,39} do not suffer from the limitations of relatively simple organic molecules. In a single-cluster junction, the electronic states of the cluster are localized on the cluster and have limited spatial overlap with the leads. 40 As a result, the probability of tunneling coherently across the entire junction is negligible. Accordingly, previous work on hexanuclear cobalt sulfide clusters demonstrated that at low biases, significant current suppression is observed due to the lack of coherent tunneling.⁴⁰ To drive a current, higher biases must be applied in order to energetically enable charging/discharging of the

Received: May 6, 2020 Published: August 18, 2020





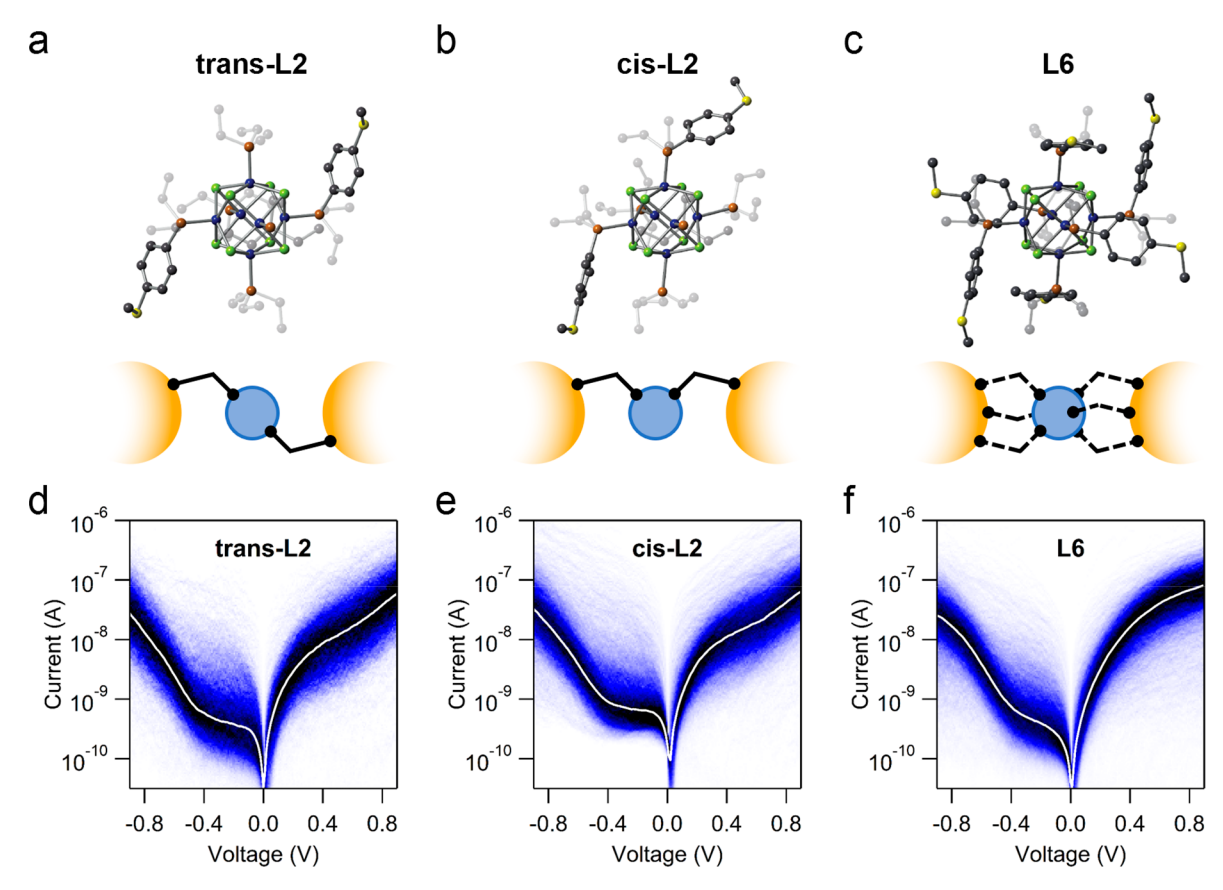


Figure 1. (a,b,c) Solid state structures of (a) trans-L2, (b) cis-L2, and (c) L6, as determined from SCXRD. Gray, blue, orange, yellow, and green spheres represent C, Co, P, S, and Se, respectively; ethyl groups are faded and H atoms are omitted for clarity. Schematic molecular junctions are also presented highlighting the differing connectivities between the cluster (blue) and the electrodes (gold). The variable connectivity of L6 is indicated with dashed lines. (d,e,f) 2D absolute current versus voltage histograms compiled from several thousand traces for (d) trans-L2 (2144 traces), (e) cis-L2 (3585 traces), and (f) L6 (4208 traces). The current is logarithmically binned (40 bins/decade), and the voltage is linearly binned (100 bins/V). The average I–V curves (white) were obtained by fitting each vertical slice of the 2D I–V histograms with a Gaussian and plotting the peak position against voltage.

cluster. ⁴¹ In this work, we elucidate the mechanism of current flow through inorganic clusters by synthesizing a series of cobalt selenide clusters of varying core sizes and surface ligand distributions. We performed room temperature current—voltage (I–V) measurements on thousands of single-cluster devices using the scanning tunneling microscope-based break junction (STM-BJ) technique. ⁴² Our results firmly establish that the mechanism of charge transport is through a sequential tunneling process. The I–V characteristics obey semiclassical heterogeneous electron transfer theory where electron transfer rates are influenced by reorganization energy. Due to their atomic precision and synthetic diversity, ^{43,44} single-cluster junctions are ideally suited to explore single-electron currents at the molecular scale toward realizing functional devices.

■ RESULTS AND DISCUSSION

In the first series of experiments, we investigate the role of device geometry on the transport properties. The clusters $[trans\text{-}Co_6Se_8(PEt_2(p\text{-}C_6H_4SMe))_2(PEt_3)_4][PF_6]$ (trans-L2), $[cis\text{-}Co_6Se_8(PEt_2(p\text{-}C_6H_4SMe))_2(PEt_3)_4][PF_6]$ (cis-L2), and $[Co_6Se_8(PEt_2(p\text{-}C_6H_4SMe))_6][BF_4]$ (L6) all contain identical $[Co_6Se_8]^{1+}$ cores but differ in the number and placement of junction-anchoring $PEt_2(p\text{-}C_6H_4SMe)$ ligands (Figure 1a–c). These anchoring ligands allow the clusters to bind to gold electrodes through thioether linkages. Although the cluster features selenium atoms, previous studies demonstrated that

junction formation does not occur without these thioether groups, confirming the necessity of these anchoring ligands. The **trans-L2** and **cis-L2** clusters exclusively enable the formation of junctions in either the *trans* or *cis* configurations, respectively. In **L6**, the cluster can bind in multiple possible configurations. By synthetically controlling the ligand positions, we can precisely engineer the geometry of the single-cluster device and probe how it affects the transport behavior.

While the synthesis and study of L6 with six identical surface ligands have been reported previously, 45 the preparation of trans-L2 and cis-L2 is only made possible by recent synthetic developments that yield substitutionally diverse yet precise clusters. 46 We synthesized and isolated, in high yields, clusters with positionally substituted carbon monoxide ligands, trans- $Co_6Se_8(CO)_2(PEt_3)_4$ and $cis-Co_6Se_8(CO)_2(PEt_3)_4$. These carbonyls are photolytically labile, and irradiation of mixtures of these precursors and PEt₂(p-C₆H₄SMe) with blue light selectively yields electrically neutral versions of trans-L2 and cis-L2. The single crystal X-ray diffraction (SCXRD) structures of the air-stable monocations of trans-L2, cis-L2, and L6, obtained via oxidation using ferrocenium, are shown in Figure 1a-c (see Figure S1 and Table S1 for more details). Despite differing surface ligands, these clusters have nearly identical physical and electronic properties. Crystal structures indicate that the cluster cores are structurally similar with negligible differences in Co-Co and Co-Se bond lengths or

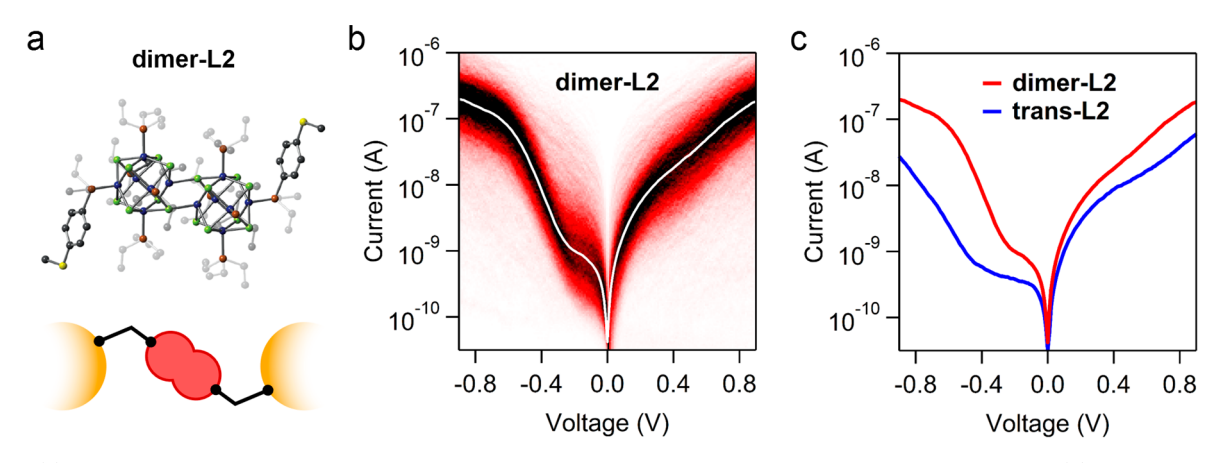


Figure 2. (a) Solid state structure of dimer-L2 as determined from SCXRD as well as a schematic molecular junction. (b) 2D absolute current versus voltage histogram for dimer-L2 compiled from 4355 traces. The current is logarithmically binned (40 bins/decade) and the voltage is linearly binned (100 bins/V). Average I–V curve is overlaid in white. (c) Average I–V curves representing most probable current versus voltage for trans-L2 (blue) and dimer-L2 (red).

the maximum S···S distances. Furthermore, cyclic voltammetry (CV) of each cluster show identical reversible redox processes at similar potentials (Figure S2).

We formed single-cluster junctions of trans-L2, cis-L2, and L6 with $\sim 1 \mu M$ solutions in propylene carbonate using the STM-BJ technique as described previously.⁴⁷ Briefly, a gold STM tip is brought in contact with a gold substrate ($\sim 1 \text{ cm}^2$) and subsequently retracted. Upon tip retraction, the gold-gold contact undergoes necking and ultimately ruptures, yielding two nanoscopic electrodes separated by ~1 nm. A single cluster from the surrounding solution can bridge the two electrodes via the anchoring ligands, thereby establishing a single-cluster junction through which current is measured. Measurements are performed on thousands of single-cluster junctions by repeatedly smashing and withdrawing the STM tip from the substrate. In order to suppress background ionic current of the solvent, we coat the tip with an insulating wax;⁴⁸ this leaves an exposed surface area of $\sim 10 \ \mu \text{m}^2$. As a consequence of the large difference in the surface areas of the tip and substrate electrodes, the voltage drop across the junction is asymmetric, and the redox levels of the cluster are effectively pinned to the chemical potential of the substrate. This allows the potential applied to the tip to dictate the charge state of the cluster. 49,50 2D histograms of standard conductance measurements of trans-L2, cis-L2, and L6 are presented in Figure S3.

To obtain the I-V characteristics, a single cluster was held between the tip and substrate at a constant distance and the current was recorded while the voltage was swept between +1 V and -1 V at a rate of 40 mV/ms (Figure S4). Several thousand I-V traces were collected for trans-L2 (Figure 1d), cis-L2 (Figure 1e), and L6 (Figure 1f). All three clusters yield similar nonlinear I-V characteristics with a distinguishable current plateau feature spanning from 0.0 to -0.4 V. These results represent a significant deviation from traditional singlemolecule devices that conduct through a coherent tunneling mechanism. When tunneling across a single-molecule junction is coherent, changing the substitution pattern, e.g., meta- vs para-substituted benzene, in general, yields different electronic characteristics.⁵¹ The similarity in the I–V characteristics for trans-L2 and cis-L2 (Figure 1d,e) provides strong evidence for an incoherent transport mechanism, that is, a mechanism in which the electron relaxes on the cluster as it transits the

junction. Additionally, the I–V characteristics of L6 are comparable to those of trans-L2 and cis-L2 (Figure 1f). These data suggest that despite there being several binding modes available to the system, the charge transport mechanism is unchanged. These results demonstrate that the ${\rm Co}_6{\rm Se}_8$ cores of these clusters function as ideal nanoscale circuit elements; they display identical electronic properties regardless of how they are wired in their circuits.

Next, we investigate the impact cluster size has on the I-V characteristics. Enabled by recent developments,⁵² we synthesized a larger cluster, [trans-Co₁₂Se₁₆(PEt₂(p- $C_6H_4SMe)_2(PEt_3)_8$ [PF₆] (dimer-L2). The core of dimer-L2 is a fused dimer of Co₆Se₈ octahedrons with two Co-Se intercluster bonds where a Co atom of one cluster is bound directly to a Se atom of another cluster (Figure 2a and Figure S5). In contrast to analogous structures with different metals, 53 the Co-Se intercluster bonds are shorter than the Co-Se intracluster bonds (Figure S6). As such, the individual Co₆Se₈ units are electronically linked and behave as a larger, cohesive cluster with a greater number of redox states than the monomeric clusters. CV demonstrates that the core of dimer-L2 can assume oxidation states spanning 1^- to 4^+ , 5^2 whereas all monomeric species can only assume the neutral to 3⁺ oxidation states (Figure S2).

The positions of the junction-anchoring ligands on dimer-L2 make for suitable comparison with trans-L2. We present a 2D histogram compiled from thousands of I-V measurements of dimer-L2 in Figure 2b. As with trans-L2, the I-V characteristics for dimer-L2 are highly nonlinear with a current plateau feature at low negative tip bias. However, the current plateau feature spans a smaller bias range from 0.0 to -0.2 V (versus 0.0 to -0.4 V in trans-L2). We directly compare the average I-V curves for trans-L2 and dimer-L2 in Figure 2c. In addition to the smaller current plateau feature, dimer-L2 exhibits higher currents at all biases. The same relationship is observed in standard conductance measurements, where the conductance of dimer-L2 is higher than that of trans-L2 (Figure S7). This observation is in sharp contrast to the typical off-resonant coherent tunneling mechanism where addition of repeat units to the conducting path results in a decreased conductance.⁵¹ Furthermore, at high negative tip bias, the current saturates in dimer-L2, and a second plateau emerges in the I-V curve. Both observations can be explained

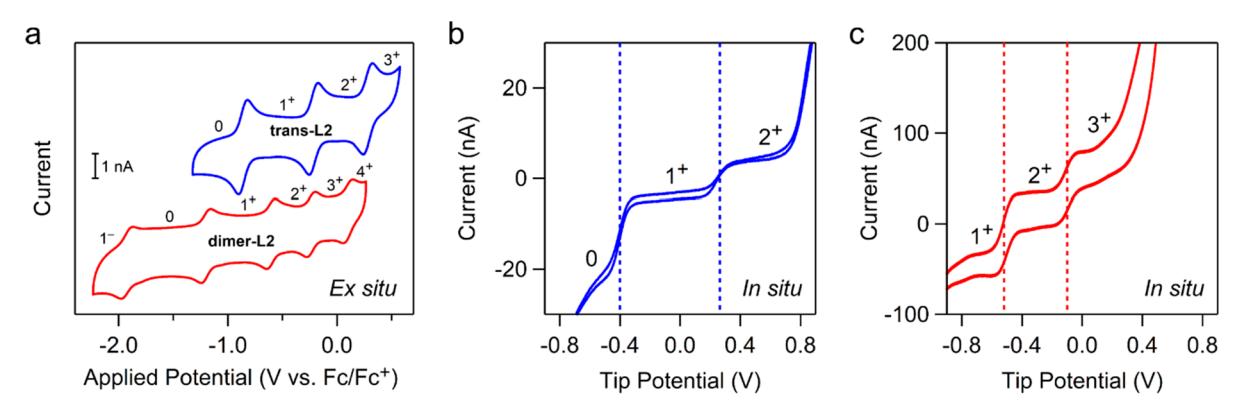


Figure 3. (a) Ex situ CV for trans-L2 (blue) and dimer-L2 (red). (b,c) In situ CV recorded for a ~ 0.1 mM solution of (b) trans-L2 and (c) dimer-L2 in PC. Current flowing into the wax-coated working electrode STM tip was measured while a linear voltage sweep (100 mV/s) was applied to the substrate. Vertical dashed lines highlight the positions of the redox transitions.

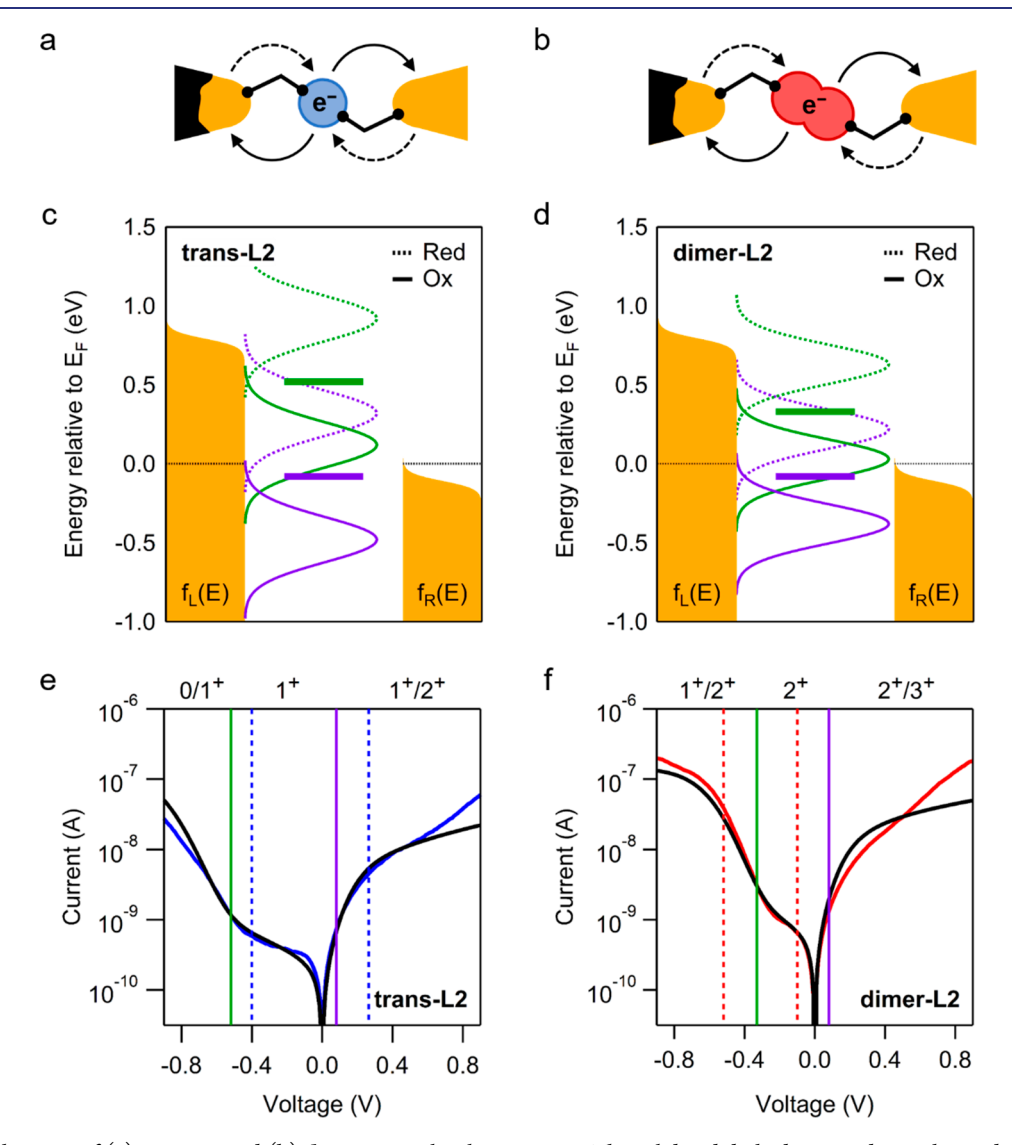


Figure 4. (a,b) Schematic of (a) **trans-L2** and (b) **dimer-L2** molecular junctions. The solid and dashed arrows depict the oxidation and reduction processes, respectively. The left electrode is the coated tip and right electrode is the substrate. (c,d) Schematic of the two-level model (i = 1, purple; i = 2, green) used to fit the I–V of (c) **trans-L2** and (d) **dimer-L2**. The Gaussian functions $D_i^{\pm}(E)$ are included in the schematic as well. The width of the Gaussians for **dimer-L2** are narrower due to the smaller reorganization energy. (e,f) Comparison of model fit (black) to experimental I–V curve for (e) **trans-L2** (blue) and (f) **dimer-L2** (red), with the oxidation state(s) for the cluster indicated. The vertical solid lines represent the values of E_1 (purple) and E_2 (green) from the model fit, and the vertical dashed lines represent the experimental redox transitions from Figure 3b,c. The spacing of the redox transitions are in good agreement between the model fit and experiment.

by a sequential incoherent tunneling mechanism and the electronic and structural properties of the larger dimer-L2. As detailed later, the dimeric cluster features smaller reorganization energies upon charging/discharging, which results in a higher current.

To explore the relationship between the transport properties and the redox properties, we performed in situ CV measurements using the STM-BJ setup for both trans-L2 and dimer-L2. The measurements were carried out with ~0.1 mM solutions of the clusters in propylene carbonate with the waxcoated gold tip withdrawn from the gold substrate. This setup functions as a two electrode electrochemical cell where the tip acts as a microscale working electrode and the substrate acts as the counter electrode.⁵⁴ Both clusters exhibit two reversible redox transitions within the bias window relevant to the I-V measurements. The in situ CV is consistent with the ex situ CV, and the redox states can be assigned (Figure 3). Note that since the in situ CV does not have a reference electrode, only the relative redox potentials should be considered as the absolute potentials may shift. Importantly, the difference between the redox transitions agree well with the bias range of the current plateau observed for both trans-L2 and dimer-L2. At low bias, within the current plateau region, trans-L2 is in the 1+ oxidation state and dimer-L2 is in the 2+ oxidation state. As the bias is increased outside of the plateau region, oxidation or reduction of the clusters is enabled and a nonlinear increase in current occurs (Figure S8). Since the electrochemical window for the 2+ oxidation state of dimer-L2 $(\Delta E \sim 0.42 \text{ eV})$ is smaller than that for the 1⁺ oxidation state of trans-L2 ($\Delta E \sim 0.66$ eV), the I–V for dimer-L2 displays a shorter current suppression plateau.

The charge transport behavior of these clusters can be described by a well-established model for hopping transport 41,55,56 derived from heterogeneous electron transfer theory. 57,58 For the semiclassical Gerischer-Hopfield model, $^{59-61}$ the rate of electron transfer for an electron of energy E between a metal and molecule for redox level i is characterized by a Gaussian function 58

$$D_i^{\pm}(E) = \frac{1}{\sqrt{4\pi\lambda_i k_{\rm B}T}} \text{Exp} \left[-\frac{(E - (E_i \pm \lambda_i))^2}{4\lambda_i k_{\rm B}T} \right]$$
(1)

where E_i is energy of the redox transition and λ_i is the reorganization energy. $(E_i + \lambda_i)$ denotes adding an electron to molecule (reduction), and $(E_i - \lambda_i)$ denotes removing an electron from the molecule (oxidation). ^{62–65}

Sequential tunneling across a molecular junction can be modeled by a set of rates of hopping on and off the cluster from both the left (L) and right (R) electrodes (Figure 4a,b). The rate of hopping on the cluster from one of the electrodes (reduction) is given by $^{41,66-68}$

$$k_{i,L(R)}^{+} = \frac{2\pi}{\hbar} \int_{-\infty}^{\infty} |t(E)|^{2} \rho_{L(R)}(E) f_{L(R)}(E) D_{i}^{+}(E) dE$$
 (2)

where $f_{L(R)}(E) = [1 + e^{(E-\mu_{L(R)})/k_BT}]^{-1}$ is the Fermi–Dirac distribution, t(E) is the tunneling matrix element, and $\rho_{L(R)}(E)$ and $\mu_{L(R)}$ are the density of states and chemical potential of the electrodes, respectively. Similarly, the rate of hopping off the cluster to one of the electrodes (oxidation) is given by

$$k_{i,L(R)}^{-} = \frac{2\pi}{\hbar} \int_{-\infty}^{\infty} |t(E)|^{2} \rho_{L(R)}(E) [1 - f_{L(R)}(E)] D_{i}^{-}(E) dE$$

We modeled the I–V characteristics of **trans-L2** and **dimer-L2** using two redox levels (i = 1, 2) in accordance with the two redox transitions observed in each *in situ* CV (Figure 4c,d). The hopping rates for the two-level model (three charge states) can be incorporated into a master equation which can be used to calculate the steady-state current as a function of applied voltage, given by 41,69,70

$$I(V) = e(k_{2,L}^{-}P(2) - k_{2,L}^{+}P(1) + k_{1,L}^{-}P(1) - k_{1,L}^{+}P(0))$$
(4)

where P(n) is the ensemble distribution of the number of electrons (n) occupying the model cluster and e is the charge of the electron (see SI Section 2).⁷¹

The fits to the experimental I-V curves are presented for trans-L2 (Figure 4e) and dimer-L2 (Figure 4f), showing excellent agreement to the experimental data. The positions of the two redox levels are demarcated by the solid vertical lines. These values relative to the Fermi energy (E_F) are $E_1 = -0.08$ eV, $E_2 = 0.52$ eV for trans-L2 and $E_1 = -0.08$ eV, $E_2 = 0.33$ eV for dimer-L2. For comparison, the positions of the redox levels from Figure 3b,c are demarcated by the dashed vertical lines. The spacing between the model levels for both trans-L2 (E_2 – $E_1 = 0.60 \text{ eV}$) and dimer-L2 ($E_2 - E_1 = 0.41 \text{ eV}$) are consistent with the *in situ* CV data ($\Delta E = 0.66$ eV for trans-L2 and $\Delta E = 0.42$ eV for dimer-L2). Note that shifts in the redox potentials from in situ CV are reasonable due to the lack of a reference electrode. Information about the absolute redox potentials comes from the ex situ CV, which indicates nearly identical oxidation potentials for [trans-L2]1+ and [dimer-L2]²⁺ (Figure 3a). Therefore, the use of $E_1 = -0.08$ eV for both trans-L2 and dimer-L2 is justified. We note that the model deviates from the experimental data at large positive tip biases. This may be due contributions to the current from higher oxidative redox transitions that are unaccounted for in this simplified two redox level model.

The values used for the reorganization energies are also within what is expected for molecular clusters: 72,73 $\lambda_{1(2)} = 0.4$ eV for trans-L2 and $\lambda_{1(2)} = 0.3$ eV for dimer-L2. The smaller reorganization energy for the larger cluster dimer-L2 is consistent with the notion that the cluster with more atoms should undergo smaller structural distortions as a response to a change in redox state. Ex situ, the reorganization energy can be shown indirectly from the changes in average Co-Co bond lengths upon oxidation or reduction. In the Co₆Se₈ core of trans-L2, for every oxidation of the cluster, an average contraction of ~0.04 Å is observed from crystal structure analysis (Figure S9). 40 By contrast, the dimer-L2 core shows no discernible change in cluster bond lengths over these oxidation states, fully consistent with the results from the fits to the model. 52 The modeling demonstrates that the increase in current for dimer-L2 can be ascribed to the smaller reorganization energy, which is in agreement with previous

In addition to higher currents, **dimer-L2** exhibits current saturation at high negative bias (Figure 2b). This current saturation is also reproduced by the model (Figure 4f). For the model, the maximum current that can be driven through the junction is given by⁴¹

$$I^{sat} = \frac{2\pi e}{\hbar} \rho(E_F) |t|^2 \tag{5}$$

where we have assumed that $t(E) \approx t$ and that $\rho_{L(R)}(E) \approx \rho(E_F)$, which is reasonable for gold electrodes. ⁶⁸ The current

saturation I^{sat} is a manifestation of the inverted Marcus regime in the context of heterogeneous electron transfer, whereby excessively energetic electrons hop onto the cluster at an increasingly slower rate. 22,54 Since trans-L2 and dimer-L2 utilize the same anchoring ligand, i.e., the same t, the same current saturation is expected for both molecular junctions. A value of $I^{sat} = 3 \times 10^{-7}$ A is used to model both trans-L2 and dimer-L2, as this value fits the data best. For trans-L2, the current saturation is not observable within the experimentally accessible bias window. However, for dimer-L2, due to its smaller reorganization energy (λ_2) and smaller reduction potential (E_2) , we are able observe a plateau in the current at large negative biases. Accordingly, dimer-L2 exhibits a higher on/off ratio than trans-L2. In a comparison of the current at -0.15 V ("off") and -0.9 V ("on"), the on/off ratios are 78 and 230 for trans-L2 and dimer-L2, respectively.

To validate I^{sat} , we can independently assess its value by estimating the tunneling matrix element (t). An approximate relationship between the low bias conductance of the anchoring ligand and the tunneling matrix element is shown in eq 6, where $G_0 = 2e^2/h$ is the quantum of conductance⁷⁷

$$G_{ligand} \approx 4\pi^2 \rho_L(E_F) \rho_R(E_F) |t|^2 G_0 \tag{6}$$

The conductance of the anchoring ligand (G_{ligand}) has been directly measured using the STM-BJ technique: $G \sim 5 \times 10^{-3}G_0$. Using $\rho_{L(R)}(E_F) = 0.3 \text{ eV}^{-1}$ for gold^{68,78} yields a value for the tunneling matrix element of t = 37.4 meV, which corresponds to a saturation current $F^{at} = 6.4 \times 10^{-7}A$ using eq 5. This estimate is in good agreement with the saturation current observed experimentally for dimer-L2 as well as the value used in the models ($F^{at} = 3 \times 10^{-7}A$).

Lastly, the I-V characteristics for trans-L2 and dimer-L2 are not only highly nonlinear but also asymmetric, with rectification ratios of 10 for trans-L2 and 6 for dimer-L2 at ±250 mV. Symmetry between the forward and reverse currents is broken by the coated tip which establishes an asymmetric ionic environment in a polar solvent.⁷⁹ We can model the influence of the coated tip by means of a voltage division factor, $0 < \eta < 1$, that describes the asymmetric voltage drop resulting from the asymmetric ionic environment. 41,80,81 The voltage division factor (or lever arm²²) is incorporated into the chemical potentials of the left and right leads as $\mu_L = E_F - \eta eV$ and $\mu_R = E_F + (1 - \eta) \text{eV}$, respectively. When $\eta = 0$, the voltage drops at the right electrode, whereas when $\eta = 1$, the voltage drops at the left electrode. Here, the left electrode represents the coated tip (Figure 4a,b), and a value of $\eta = 0.88$ is found to fit the data best. This agrees with the assumption that due to the small surface area of the tip electrode, most of the voltage drops between tip and the molecule. 50 In Figure 4c,d, the chemical potentials of the tip (μ_L) and substrate (μ_R) are depicted for a 0.9 V bias with η = 0.88. We note that the coated tip alone does not yield current rectification. The current rectification observed for the clusters measured herein results from the asymmetric positions of the redox levels relative to E_F. In contrast, no current rectification was observed for previously measured Co₆S₈ clusters, for which the redox levels were equally separated from E_F.4

CONCLUSIONS

We have studied the charge transport properties of atomically precise inorganic clusters with varying surface ligand structure and core composition. The identical transport behaviors of trans-L2, cis-L2, and L6, as well as agreement with a model drawn from Marcus theory, firmly establish a sequential tunneling mechanism. Current is driven in these devices via an electron tunneling from the source electrode to the cluster through one anchoring ligand and then a sequential tunneling step to the drain electrode via another anchoring ligand. An increase in the cluster core size from trans-L2 to dimer-L2 yields higher currents due to a reduction in both the reorganization energies and the energetic separation of the charge states. Additionally, dimer-L2 exhibits current saturation at large negative bias, which further substantiates the proposed Marcus-based transport mechanism.

The single cluster devices exhibit practically relevant properties including nonlinear I–V characteristics and current rectification, and our work establishes design principles through which these device properties can be engineered. By modifying the anchoring ligand or cluster composition through synthetic chemistry, one can tune the position and width of the current suppression plateau, the nonlinearity of the I–V, as well as the extent of current rectification. Moreover, the single-electron character of the devices opens up the possibility of performing room temperature single-electron manipulations in a molecular junction. Lastly, with an increase in the cluster size beyond dimer-L2, the transition from discrete molecule to extended material can be explored.

ASSOCIATED CONTENT

Supporting Information

The Supporting Information is available free of charge at https://pubs.acs.org/doi/10.1021/jacs.0c04970.

(CIF)

Experimental methods, model details, and figures (PDF) (CIF)

(CIF)

AUTHOR INFORMATION

Corresponding Authors

Latha Venkataraman — Department of Chemistry and Department of Applied Physics and Applied Mathematics, Columbia University, New York, New York 10027, United States; Occid.org/0000-0002-6957-6089; Email: lv2117@columbia.edu

Michael L. Steigerwald — Department of Chemistry, Columbia University, New York, New York 10027, United States; Email: mls2064@columbia.edu

Xavier Roy — Department of Chemistry, Columbia University, New York, New York 10027, United States; ocid.org/0000-0002-8850-0725; Email: xr2114@columbia.edu

Colin Nuckolls — Department of Chemistry, Columbia University, New York, New York 10027, United States; orcid.org/0000-0002-0384-5493; Email: cn37@columbia.edu

Authors

Suman Gunasekaran — Department of Chemistry, Columbia University, New York, New York 10027, United States;
ocid.org/0000-0001-5974-0642

Douglas A. Reed – Department of Chemistry, Columbia University, New York, New York 10027, United States; orcid.org/0000-0001-5170-9050

Daniel W. Paley – Department of Chemistry, Columbia University, New York, New York 10027, United States Amymarie K. Bartholomew – Department of Chemistry, Columbia University, New York, New York 10027, United States

Complete contact information is available at: https://pubs.acs.org/10.1021/jacs.0c04970

Author Contributions

^{\$}These authors contributed equally. The manuscript was written through contributions of all authors. All authors have given approval to the final version of the manuscript.

Notes

The authors declare no competing financial interest.

ACKNOWLEDGMENTS

Valuable discussions with E-Dean Fung and Louis E. Brus are gratefully acknowledged. Support for this research was provided by the Center for Precision Assembly of Superstratic and Superatomic Solids, an NSF MRSEC (award number DMR-1420634), and Air Force Office of Scientific Research (award number FA9550-18-1-0020). C.N. thanks Sheldon and Dorothea Buckler for their generous support. X.R. acknowledges support from the NSF CAREER program (award number NSF DMR-1751949). S.G. is supported by a NSF Graduate Research Fellowship under Grant No. DGE-1644869. D.A.R. thanks the Columbia Nano Initiative at Columbia University for postdoctoral fellowship support. Single-crystal X-ray diffraction analysis was performed at the Shared Materials Characterization Laboratory (SMCL) at Columbia University. Use of the SMCL was made possible by funding from Columbia University.

REFERENCES

- (1) Fulton, T. A.; Dolan, G. J. Observation of Single-Electron Charging Effects in Small Tunnel-Junctions. *Phys. Rev. Lett.* **1987**, *59* (1), 109–112.
- (2) Likharev, K. K. Single-electron devices and their applications. *Proc. IEEE* **1999**, 87 (4), 606–632.
- (3) Grabert, H.; Devoret, M. H.; North Atlantic Treaty Organization. Scientific Affairs Division., Single charge tunneling: Coulomb blockade phenomena in nanostructures. Plenum Press: New York, 1992; p xiii, 335 p.
- (4) Kastner, M. A. The Single-Electron Transistor. Rev. Mod. Phys. 1992, 64 (3), 849–858.
- (5) Chen, R. H.; Korotkov, A. N.; Likharev, K. K. Single-electron transistor logic. *Appl. Phys. Lett.* **1996**, *68* (14), 1954–1956.
- (6) Mills, A. R.; Zajac, D. M.; Gullans, M. J.; Schupp, F. J.; Hazard, T. M.; Petta, J. R., Shuttling a single charge across a one-dimensional array of silicon quantum dots. *Nat. Commun.* **2019**, *10*. DOI: 10.1038/s41467-019-08970-z
- (7) Buch, H.; Mahapatra, S.; Rahman, R.; Morello, A.; Simmons, M. Y. Spin readout and addressability of phosphorus-donor clusters in silicon. *Nat. Commun.* **2013**, *4*, 4.
- (8) Yang, C. H.; Leon, R. C. C.; Hwang, J. C. C.; Saraiva, A.; Tanttu, T.; Huang, W.; Camirand Lemyre, J.; Chan, K. W.; Tan, K. Y.; Hudson, F. E.; Itoh, K. M.; Morello, A.; Pioro-Ladrière, M.; Laucht, A.; Dzurak, A. S. Operation of a silicon quantum processor unit cell above one kelvin. *Nature* **2020**, *580* (7803), 350–354.
- (9) Petit, L.; Eenink, H. G. J.; Russ, M.; Lawrie, W. I. L.; Hendrickx, N. W.; Philips, S. G. J.; Clarke, J. S.; Vandersypen, L. M. K.; Veldhorst, M. Universal quantum logic in hot silicon qubits. *Nature* **2020**, *580* (7803), 355–359.
- (10) Ishikuro, H.; Hiramoto, T. Quantum mechanical effects in the silicon quantum dot in a single-electron transistor. *Appl. Phys. Lett.* **1997**, 71 (25), 3691–3693.

- (11) Kano, S.; Tada, T.; Majima, Y. Nanoparticle characterization based on STM and STS. Chem. Soc. Rev. 2015, 44 (4), 970-987.
- (12) Cheng, G. L.; Siles, P. F.; Bi, F.; Cen, C.; Bogorin, D. F.; Bark, C. W.; Folkman, C. M.; Park, J. W.; Eom, C. B.; Medeiros-Ribeiro, G.; Levy, J. Sketched oxide single-electron transistor. *Nat. Nanotechnol.* **2011**, *6* (6), 343–347.
- (13) Fuechsle, M.; Miwa, J. A.; Mahapatra, S.; Ryu, H.; Lee, S.; Warschkow, O.; Hollenberg, L. C. L.; Klimeck, G.; Simmons, M. Y. A single-atom transistor. *Nat. Nanotechnol.* **2012**, *7* (4), 242–246.
- (14) Andres, R. P.; Bein, T.; Dorogi, M.; Feng, S.; Henderson, J. I.; Kubiak, C. P.; Mahoney, W.; Osifchin, R. G.; Reifenberger, R. 'Coulomb staircase' at room temperature in a self-assembled molecular nanostructure. *Science* 1996, 272 (5266), 1323–1325.
- (15) Klein, D. L.; Roth, R.; Lim, A. K. L.; Alivisatos, A. P.; McEuen, P. L. A single-electron transistor made from a cadmium selenide nanocrystal. *Nature* **1997**, 389 (6652), 699–701.
- (16) Chen, S. W.; Ingram, R. S.; Hostetler, M. J.; Pietron, J. J.; Murray, R. W.; Schaaff, T. G.; Khoury, J. T.; Alvarez, M. M.; Whetten, R. L. Gold nanoelectrodes of varied size: Transition to molecule-like charging. *Science* **1998**, 280 (5372), 2098–2101.
- (17) Ingram, R. S.; Hostetler, M. J.; Murray, R. W.; Schaaff, T. G.; Khoury, J. T.; Whetten, R. L.; Bigioni, T. P.; Guthrie, D. K.; First, P. N. 28 kDa alkanethiolate-protected Au clusters give analogous solution electrochemistry and STM Coulomb staircases. *J. Am. Chem. Soc.* **1997**, *119* (39), 9279–9280.
- (18) Huang, C. C.; Rudnev, A. V.; Hong, W. J.; Wandlowski, T. Break junction under electrochemical gating: testbed for single-molecule electronics. *Chem. Soc. Rev.* **2015**, *44* (4), 889–901.
- (19) Sun, L.; Diaz-Fernandez, Y. A.; Gschneidtner, T. A.; Westerlund, F.; Lara-Avila, S.; Moth-Poulsen, K. Single-molecule electronics: from chemical design to functional devices. *Chem. Soc. Rev.* **2014**, *43* (21), 7378–7411.
- (20) Tsutsui, M.; Taniguchi, M. Single Molecule Electronics and Devices. Sensors 2012, 12 (6), 7259-7298.
- (21) Nichols, R. J.; Higgins, S. J. Single-Molecule Electronics: Chemical and Analytical Perspectives. *Annu. Rev. Anal. Chem.* **2015**, *8*, 389–417.
- (22) Roy-Gobeil, A.; Miyahara, Y.; Bevan, K. H.; Grutter, P. Fully Quantized Electron Transfer Observed in a Single Redox Molecule at a Metal Interface. *Nano Lett.* **2019**, *19* (9), 6104–6108.
- (23) Fatayer, S.; Schuler, B.; Steurer, W.; Scivetti, I.; Repp, J.; Gross, L.; Persson, M.; Meyer, G. Reorganization energy upon charging a single molecule on an insulator measured by atomic force microscopy. *Nat. Nanotechnol.* **2018**, *13* (5), 376.
- (24) Patera, L. L.; Queck, F.; Scheuerer, P.; Repp, J. Mapping orbital changes upon electron transfer with tunnelling microscopy on insulators. *Nature* **2019**, *566* (7743), 245.
- (25) Kubatkin, S.; Danilov, A.; Hjort, M.; Cornil, J.; Bredas, J. L.; Stuhr-Hansen, N.; Hedegard, P.; Bjornholm, T. Single-electron transistor of a single organic molecule with access to several redox states. *Nature* **2003**, 425 (6959), 698–701.
- (26) Nichols, R. J.; Higgins, S. J. Single Molecule Nanoelectrochemistry in Electrical Junctions. *Acc. Chem. Res.* **2016**, 49 (11), 2640–2648.
- (27) Chappell, S.; Brooke, C.; Nichols, R. J.; Cook, L. J. K.; Halcrow, M.; Ulstrup, J.; Higgins, S. J. Evidence for a hopping mechanism in metall single moleculel metal junctions involving conjugated metal-terpyridyl complexes; potential-dependent conductances of complexes [M(pyterpy)(2)](2+) (M = Co and Fe; pyterpy = 4 '-(pyridin-4-yl)-2,2 ':6 ',2 "-terpyridine) in ionic liquid. *Faraday Discuss.* **2016**, *193*, 113–131.
- (28) Kolivoska, V.; Valasek, M.; Gal, M.; Sokolova, R.; Bulickova, J.; Pospisil, L.; Meszaros, G.; Hromadova, M. Single-Molecule Conductance in a Series of Extended Viologen Molecules. *J. Phys. Chem. Lett.* **2013**, *4* (4), 589–595.
- (29) Higgins, S. J.; Nichols, R. J. Metal/molecule/metal junction studies of organometallic and coordination complexes; What can transition metals do for molecular electronics? *Polyhedron* **2018**, *140*, 25–34.

- (30) Solomon, G. C.; Herrmann, C.; Hansen, T.; Mujica, V.; Ratner, M. A. Exploring local currents in molecular junctions. *Nat. Chem.* **2010**, 2 (3), 223–228.
- (31) Haiss, W.; van Zalinge, H.; Higgins, S. J.; Bethell, D.; Hobenreich, H.; Schiffrin, D. J.; Nichols, R. J. Redox state dependence of single molecule conductivity. *J. Am. Chem. Soc.* **2003**, *125* (50), 15294–15295.
- (32) Zhang, F.; Wu, X. H.; Zhou, Y. F.; Wang, Y. H.; Zhou, X. S.; Shao, Y.; Li, J. F.; Jin, S.; Zheng, J. F. Improving Gating Efficiency of Electron Transport through Redox-Active Molecular Junctions with Conjugated Chains. *ChemElectroChem* **2020**, *7*, 1288.
- (33) Darwish, N.; Diez-Perez, I.; Guo, S. Y.; Tao, N. J.; Gooding, J. J.; Paddon-Row, M. N. Single Molecular Switches: Electrochemical Gating of a Single Anthraquinone-Based Norbornylogous Bridge Molecule. *J. Phys. Chem. C* **2012**, *116* (39), 21093–21097.
- (34) Schwarz, F.; Kastlunger, G.; Lissel, F.; Egler-Lucas, C.; Semenov, S. N.; Venkatesan, K.; Berke, H.; Stadler, R.; Lortscher, E. Field-induced conductance switching by charge-state alternation in organometallic single-molecule junctions. *Nat. Nanotechnol.* **2016**, *11* (2), 170–176.
- (35) Schwarz, F.; Koch, M.; Kastlunger, G.; Berke, H.; Stadler, R.; Venkatesan, K.; Lortscher, E. Charge Transport and Conductance Switching of Redox-Active Azulene Derivatives. *Angew. Chem., Int. Ed.* **2016**, *55* (39), 11781–11786.
- (36) Ruben, M.; Landa, A.; Lortscher, E.; Riel, H.; Mayor, M.; Gorls, H.; Weber, H. B.; Arnold, A.; Evers, F. Charge Transport Through a Cardan-Joint Molecule. *Small* **2008**, *4* (12), 2229–2235.
- (37) Ting, T. C.; Hsu, L. Y.; Huang, M. J.; Horng, E. C.; Lu, H. C.; Hsu, C. H.; Jiang, C. H.; Jin, B. Y.; Peng, S. M.; Chen, C. H. Energy-Level Alignment for Single-Molecule Conductance of Extended Metal-Atom Chains. *Angew. Chem., Int. Ed.* **2015**, *54* (52), 15734–15738
- (38) Pinkard, A.; Champsaur, A. M.; Roy, X. Molecular Clusters: Nanoscale Building Blocks for Solid-State Materials. *Acc. Chem. Res.* **2018**, *51* (4), 919–929.
- (39) Lin, Z. Y.; Williams, I. D. Structure and bonding in face- and edge-bridged octahedral transition metal clusters. *Polyhedron* **1996**, *15* (19), 3277–3287.
- (40) Lovat, G.; Choi, B.; Paley, D. W.; Steigerwald, M. L.; Venkataraman, L.; Roy, X. Room-temperature current blockade in atomically defined single-cluster junctions. *Nat. Nanotechnol.* **2017**, *12* (11), 1050.
- (41) Migliore, A.; Nitzan, A. Nonlinear Charge Transport in Redox Molecular Junctions: A Marcus Perspective. *ACS Nano* **2011**, *5* (8), 6669–6685.
- (42) Xu, B. Q.; Tao, N. J. J. Measurement of single-molecule resistance by repeated formation of molecular junctions. *Science* **2003**, 301 (5637), 1221–1223.
- (43) McCleverty, J. A.; Meyer, T. J. Comprehensive coordination chemistry II: from biology to nanotechnology. 1st ed.; Elsevier Pergamon: Amsterdam; Boston, 2004.
- (44) Fedorov, V. E.; Mishchenko, A. V.; Fedin, V. P. Cluster Transition Metal Chalcogenide Halides. *Russ. Chem. Rev.* **1985**, *54* (4), 408–423.
- (45) Roy, X.; Schenck, C. L.; Ahn, S.; Lalancette, R. A.; Venkataraman, L.; Nuckolls, C.; Steigerwald, M. L. Quantum Soldering of Individual Quantum Dots. *Angew. Chem., Int. Ed.* **2012**, *S1* (50), 12473–12476.
- (46) Champsaur, A. M.; Velian, A.; Paley, D. W.; Choi, B.; Roy, X.; Steigerwald, M. L.; Nuckolls, C. Building Diatomic and Triatomic Superatom Molecules. *Nano Lett.* **2016**, *16* (8), 5273–5277.
- (47) Venkataraman, L.; Klare, J. E.; Tam, I. W.; Nuckolls, C.; Hybertsen, M. S.; Steigerwald, M. L. Single-molecule circuits with well-defined molecular conductance. *Nano Lett.* **2006**, *6* (3), 458–462.
- (48) Nagahara, L. A.; Thundat, T.; Lindsay, S. M. Preparation and Characterization of Stm Tips for Electrochemical Studies. *Rev. Sci. Instrum.* **1989**, *60* (10), 3128–3130.

- (49) Capozzi, B.; Low, J. Z.; Xia, J. L.; Liu, Z. F.; Neaton, J. B.; Campos, L. M.; Venkataraman, L. Mapping the Transmission Functions of Single-Molecule Junctions. *Nano Lett.* **2016**, *16* (6), 3949–3954.
- (50) Capozzi, B.; Xia, J. L.; Adak, O.; Dell, E. J.; Liu, Z. F.; Taylor, J. C.; Neaton, J. B.; Campos, L. M.; Venkataraman, L. Single-molecule diodes with high rectification ratios through environmental control. *Nat. Nanotechnol.* **2015**, *10* (6), 522–U101.
- (51) Su, T. A.; Neupane, M.; Steigerwald, M. L.; Venkataraman, L.; Nuckolls, C. Chemical principles of single-molecule electronics. *Nat. Rev. Mater.* **2016**, *1* (3), 3.
- (52) Champsaur, A. M.; Hochuli, T. J.; Paley, D. W.; Nuckolls, C.; Steigerwald, M. L. Superatom Fusion and the Nature of Quantum Confinement. *Nano Lett.* **2018**, *18* (7), 4564–4569.
- (53) Amari, S.; Imoto, H.; Saito, T. Synthesis and structures of [Mo12E16(PEt3)(10)] (E = S, Se). *J. Chin. Chem. Soc.* **1998**, 45 (4), 445–450.
- (54) Bard, A. J.; Faulkner, L. R. Electrochemical methods: fundamentals and applications. Wiley: New York, 1980; p xviii, 718 p.
- (55) Kuznetsov, A. M.; Ulstrup, J. Electron transfer in chemistry and biology: an introduction to the theory. Wiley: Chichester; New York, 1999; p xvi, 357 p.
- (56) Kuznetsov, A. M.; Medvedev, I. G.; Ulstrup, J. Coulomb repulsion effect in two-electron nonadiabatic tunneling through a one-level redox molecule. *J. Chem. Phys.* **2009**, *131* (16), 164703.
- (57) Hush, N. S. Adiabatic Rate Processes at Electrodes 0.1. Energy-Charge Relationships. *J. Chem. Phys.* **1958**, 28 (5), 962–972.
- (58) Marcus, R. A. Chemical and electrochemical electron-transfer theory. *Annu. Rev. Phys. Chem.* **1964**, *15* (1), 155–196.
- (59) Hopfield, J. J. Electron-Transfer between Biological Molecules by Thermally Activated Tunneling. *Proc. Natl. Acad. Sci. U. S. A.* **1974**, 71 (9), 3640–3644.
- (60) Gerischer, H. The Impact of Semiconductors on the Concepts of Electrochemistry. *Electrochim. Acta* **1990**, 35 (11–12), 1677–1699.
- (61) Bevan, K. H., Electron transfer from the perspective of electron transmission: Biased non-adiabatic intermolecular reactions in the single-particle picture. *J. Chem. Phys.* **2017**, *146* (13).134106
- (62) Schmickler, W. Interfacial electrochemistry. Oxford University Press: New York, 1996; p xii, 288 p.
- (63) Bard, A. J.; Faulkner, L. R. Electrochemical methods: fundamentals and applications. 2nd ed.; Wiley: New York, 2001; p xxi, 833 p.
- (64) Schmickler, W. Current-Potential Curves in Simple Electrochemical Redox Reactions. *Electrochim. Acta* 1975, 20 (2), 137–141.
- (65) Chidsey, C. E. D. Free-Energy and Temperature-Dependence of Electron-Transfer at the Metal-Electrolyte Interface. *Science* **1991**, 251 (4996), 919–922.
- (66) Migliore, A.; Schiff, P.; Nitzan, A. On the relationship between molecular state and single electron pictures in simple electrochemical junctions. *Phys. Chem. Chem. Phys.* **2012**, *14* (40), 13746–13753.
- (67) Kuznetsov, A. M.; Ulstrup, J. Theory of electron transfer at electrified interfaces. *Electrochim. Acta* **2000**, 45 (15–16), 2339–2361
- (68) Adams, D. M.; Brus, L.; Chidsey, C. E.; Creager, S.; Creutz, C.; Kagan, C. R.; Kamat, P. V.; Lieberman, M.; Lindsay, S.; Marcus, R. A. Charge transfer on the nanoscale: current status. *J. Phys. Chem. B* **2003**, *107* (28), 6668–6697.
- (69) Muralidharan, B.; Datta, S., Generic model for current collapse in spin-blockaded transport. *Phys. Rev. B: Condens. Matter Mater. Phys.* **2007**, 76 (3). DOI: 10.1103/PhysRevB.76.035432
- (70) Kuznetsov, A. M.; Medvedev, I. G. Effect of Coulomb interaction between the electrons on two-electron redox-mediated tunneling. *Electrochem. Commun.* **2008**, *10* (8), 1191–1194.
- (71) Hanna, A. E.; Tinkham, M. Variation of the Coulomb Staircase in a 2-Junction System by Fractional Electron Charge. *Phys. Rev. B: Condens. Matter Mater. Phys.* **1991**, 44 (11), 5919–5922.
- (72) Antonello, S.; Perera, N. V.; Ruzzi, M.; Gascon, J. A.; Maran, F. Interplay of Charge State, Lability, and Magnetism in the Molecule-

- like Au-25(SR)(18) Cluster. J. Am. Chem. Soc. 2013, 135 (41), 15585-15594.
- (73) Sigfridsson, E.; Olsson, M. H. M.; Ryde, U. Inner-sphere reorganization energy of iron-sulfur clusters studied with theoretical methods. *Inorg. Chem.* **2001**, *40* (11), 2509–2519.
- (74) Zhang, W.; Gan, S. Y.; Vezzoli, A.; Davidson, R. J.; Milan, D. C.; Luzyanin, K. V.; Higgins, S. J.; Nichols, R. J.; Beeby, A.; Low, P. J.; Li, B. Y.; Niu, L. Single-Molecule Conductance of Viologen-Cucurbit[8]uril Host-Guest Complexes. *ACS Nano* **2016**, *10* (5), 5212–5220.
- (75) Zhou, X. S.; Liu, L.; Fortgang, P.; Lefevre, A. S.; Serra-Muns, A.; Raouafi, N.; Amatore, C.; Mao, B. W.; Maisonhaute, E.; Schollhorn, B. Do Molecular Conductances Correlate with Electrochemical Rate Constants? Experimental Insights. *J. Am. Chem. Soc.* **2011**, *133* (19), 7509–7516.
- (76) Kastlunger, G.; Stadler, R. Density functional theory based direct comparison of coherent tunneling and electron hopping in redox-active single-molecule junctions. *Phys. Rev. B: Condens. Matter Mater. Phys.* **2015**, 91 (12), 12.
- (77) Mujica, V.; Kemp, M.; Ratner, M. A. Electron Conduction in Molecular Wires 0.1. A Scattering Formalism. *J. Chem. Phys.* **1994**, 101 (8), 6849–6855.
- (78) Royea, W. J.; Fajardo, A. M.; Lewis, N. S. Fermi golden rule approach to evaluating outer-sphere electron-transfer rate constants at semiconductor/liquid interfaces. *J. Phys. Chem. B* **1997**, *101* (51), 11152—11159
- (79) Cheung, K. C. M.; Chen, X. Y.; Albrecht, T.; Kornyshev, A. A. Principles of a Single-Molecule Rectifier in Electrolytic Environment. *J. Phys. Chem. C* **2016**, 120 (6), 3089–3106.
- (80) Datta, S.; Tian, W. D.; Hong, S. H.; Reifenberger, R.; Henderson, J. I.; Kubiak, C. P. Current-voltage characteristics of self-assembled monolayers by scanning tunneling microscopy. *Phys. Rev. Lett.* **1997**, *79* (13), 2530–2533.
- (81) Tian, W. D.; Datta, S.; Hong, S. H.; Reifenberger, R.; Henderson, J. I.; Kubiak, C. P. Conductance spectra of molecular wires. *J. Chem. Phys.* **1998**, *109* (7), 2874–2882.